



Robotic swimming in curved space via geometric phase

Shengkai Li^{a,1} , Tianyu Wang^{a,b,1} , Velin H. Kojouharov^c, James McInerney^d, Enes Aydin^e, Yasemin Ozkan-Aydin^f , Daniel I. Goldman^a , and D. Zeb Rocklin^{a,2}

Edited by John Rogers, Northwestern University, Evanston, IL; received January 18, 2022; accepted June 24, 2022

Locomotion by shape changes or gas expulsion is assumed to require environmental interaction, due to conservation of momentum. However, as first noted in [J. Wisdom, *Science* 299, 1865–1869 (2003)] and later in [E. Guérin, *Sci. Am.* 301, 38–45 (2009)] and [J. Avron, O. Kenneth, *New J. Phys.* 8, 68 (2006)], the noncommutativity of translations permits translation without momentum exchange in either gravitationally curved spacetime or the curved surfaces encountered by locomotors in real-world environments. To realize this idea which remained unvalidated in experiments for almost 20 y, we show that a precision robophysical apparatus consisting of motors driven on curved tracks (and thereby confined to a spherical surface without a solid substrate) can self-propel without environmental momentum exchange. It produces shape changes comparable to the environment's inverse curvatures and generates movement of 10^{-1} cm per gait. While this simple geometric effect predominates over short time, eventually the dissipative (frictional) and conservative forces, ubiquitous in real systems, couple to it to generate an emergent dynamics in which the swimming motion produces a force that is counter-balanced against residual gravitational forces. In this way, the robot both swims forward without momentum and becomes fixed in place with a finite momentum that can be released by ceasing the swimming motion. We envision that our work will be of use in a broad variety of contexts, such as active matter in curved space and robots navigating real-world environments with curved surfaces.

active matter | manifold | curvature | geometric phase | emergent dynamics

Curved surfaces are ubiquitous in physics, biology, engineering, and mathematics but are defined by features that defy intuitions derived from flat space. For example, on a spherical surface, the square of the hypotenuse is not the sum of the squares of the legs, “parallel” lines meet at the poles, and the sum of the interior angles of a triangle grows with the triangle's area. These geometric (and topological) effects can profoundly alter conventional dynamics, as when the inability to form periodic crystals on spherical surfaces (1, 2) recently gave rise to lively dynamics of essential crystalline defects (3, 4). Geometric frustrated extended objects in curved space have been found to move due to the stress from the incompatibility (5). Additionally, of course, gravitational interactions themselves are derived from the fundamental curvature of four-dimensional space-time (6), leading to explanations of dynamics, such as the precessing orbit of Mercury and the gravitational lensing of light.

Less well known is the fact that curved surfaces permit locomotors embedded within them to self-propel via translation without exchanging momentum with an environment (7–9) (as is done in swimming, flying, and running in typical environments). How can this be? Consider, in particular, the prototypical swimmer confined to (or embedded within) the spherical surface depicted in Fig. 1A. By propelling masses along the vertical arms, the component of the moment of inertia that relates torque and angular momentum about the longitudinal axis, which are particular cases of the concepts of generalized force and momentum, can be altered, analogous to a process in flat space that somehow altered the mass of an object. By propelling an additional mass along the latitudinal arm on the sphere, angular momentum may be exchanged between this mass and the others during periods in which the robot has different moments of inertia. By pushing itself in one direction when it has low moment of inertia and the other when it has high, the robot may attain a net movement in the first direction, even as the total robot structure maintains zero angular momentum. This is analogous to a falling cat, which instinctively exchanges angular momentum between different parts of its body while contorting itself to alter its moment of inertia.

This process relates to fundamental geometric properties. Whereas a flat plane is invariant under two translations and a rotation, leading to a two-dimensional conserved linear momentum and a one-dimensional conserved angular momentum, a spherical surface is invariant under the three rigid-body rotations of SO(3) (special orthogonal group 3, i.e. 3D rotation group), leading to a conserved three-dimensional (3D) angular momentum.

Significance

In Newtonian dynamics, acceleration requires force, which is taken to imply that a stationary object cannot move without exchanging momentum with its environment. Here, we realize a system that defies this requirement: a robot confined to a sphere. As the device actively changes its shape, the noncommutativity of “translations” in curved spaces allows it to advance without frictional or gravitational forces, akin to how a falling cat can use shape changes to control its orientation but not its position. Under controlled frictional forces, the robot can achieve a state with finite momentum that nevertheless does not move forward. Our work demonstrates how the interaction between environmental curvature, active driving, and geometric phases yields rich, exotic phenomena.

Author contributions: J.M., E.A., Y.O.-A., D.I.G., and D.Z.R. designed research; S.L., T.W., and V.H.K. performed research; S.L., T.W., J.M., and D.Z.R. contributed new reagents/analytic tools; S.L., T.W., and V.H.K. analyzed data; and S.L., T.W., J.M., D.I.G., and D.Z.R. wrote the paper.

The authors declare no competing interest.

This article is a PNAS Direct Submission.

Copyright © 2022 the Author(s). Published by PNAS. This article is distributed under Creative Commons Attribution-NonCommercial-NoDerivatives License 4.0 (CC BY-NC-ND).

¹S.L. and T.W. contributed equally to this work.

²To whom correspondence may be addressed. Email: zebrocklin@gatech.edu.

This article contains supporting information online at <https://www.pnas.org/lookup/suppl/doi:10.1073/pnas.2200924119/-DCSupplemental>.

Published July 28, 2022.

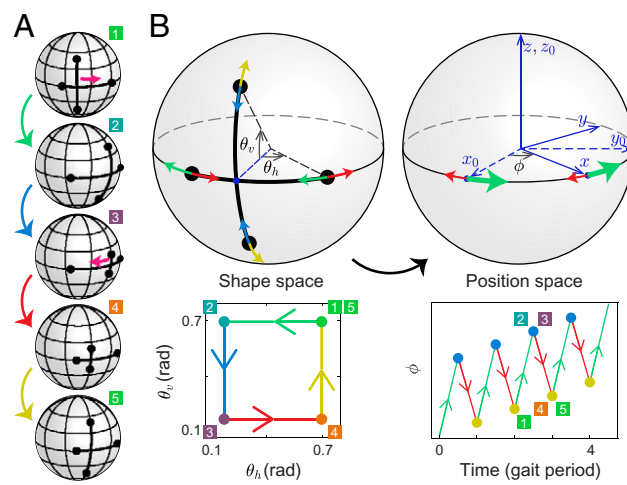


Fig. 1. Self-propulsion without reaction forces. (A) A robot confined to a spherical surface executes a cyclic change of shape to generate net position change. (B) The cyclic change of shape described by the angles θ_h , θ_v of motorized weights (black dots) follows an order indicated by the gait diagram in Lower. Due to the variable moment of inertia and the noncommutativity of these operations, this leads to a net change in the robot's position, represented by the rotation $\phi(t)$ applied to the coordinate axes in position space, even in the absence of momentum or external forces. The plot in Lower shows the time evolution of $\phi(t)$ from each stroke of the gait shown in the same color as the gait diagram.

Crucially, these motions, which may be thought of as translations along the sphere, do not commute with each other as do translations in flat space. Consequently, when a robot changes its shape on a sphere as shown in Fig. 1A, it induces a series of incommensurate motions, so that a closed cycle of shapes induces a net displacement along the sphere, analogous to the rotation achieved by a falling cat.

This behavior is an example of a broader phenomenon in physics, in which dynamically varying patterns can induce a physical transformation known as a geometric phase. Geometric phase plays a crucial role in modern physics from the general relativistic curvature of space-time that establishes closed orbits of planets around stars to the Berry curvature that underlies quantum-mechanical effects in graphene, topological insulators, and cyclotron motion. Additionally, geometric phase even appears in locomotion. As pointed out by Shapere and Wilczek (10) and developed and applied over the past decades (11–16), geometric phase describes how a self-deforming body locomotes in response to drag forces from viscous and frictional fluids to dry friction. Hannay (17), building on earlier work by Saffman (18), likewise demonstrated that swimming in Euler fluids, dominated by inertial effects, is captured via a geometrical phase.

Here, we demonstrate experimentally geometric phase driving dynamics solely induced by the curvature of space, resulting in self-propulsion without environmental force exchange. A straightforward method would be confining an extended object to a spherical substrate that does not generate significant forces overwhelming the desired effect. Nonetheless, it is challenging to achieve in this way without introducing Earth's gravity and tangential constraining force, and this could be the reason that the concept of swimming on curved space has been left unvalidated experimentally for almost two decades. Therefore, we take a different route by converting the abstract picture of the ideal spherical surface swimmer mentioned above to a precision robophysical model. The device's self-propulsion is determined by the geometrical phase induced by its shape changes as it slides motorized masses along curved tracks.

Further, under complex dissipative coupling to the environment, this geometric propulsion couples to friction in surprising ways, preventing decay into energy minima of external field and capturing a finite-momentum state in a fixed position. Given the ubiquity of dissipation and external fields in realistic systems, we envision that our result will be helpful in understanding active matter on curved surfaces (19, 20) and robots navigating real-world environments with curved surfaces [e.g., self-propelling robots on deformable membranes (21)].

Shape Change Dynamics in Curved Space

Testing the idea that self-propulsion can occur in curved environments without forces requires confining the robophysical model to a curved surface while achieving control over its environmental coupling. While experiments often occur in flat planes whose dynamics approximate that of an ideal Euclidean plane, capturing the essence of a sphere is more challenging. In particular, no widely available method exists for placing particles on a solid spherical shell while simultaneously minimizing both the effect of gravity (which would drive particles toward the bottom of the sphere) and friction (which would prevent us from isolating the curvature-induced motion from more conventional effects). Instead, we opt for a solution in which we attach the robot to a rigid boom arm free only to rotate about the vertical axis, as shown in Fig. 2A.

Masses are robotically propelled along curved tracks whose radius coincides with the length of the boom arm, ensuring that the robot's mass is confined to a spherical surface. The constraint of the boom arm ensures that all forces/torques that would move the robot vertically or radially are negated while freely permitting horizontal direction along the spherical surface. Consequently, the dynamics of the apparatus is well described by that of an ideal sphere. Notably, the robot's ability to move does not violate the usual rule against movement without forces in 3D space because the full 3D dynamics in fact includes normal forces on the robot supplied by the boom arm that confines it to the sphere.

This arrangement is achieved via precision servo motors connected to gears that move without slipping on the robot's 3D printed toothed tracks that can be generated with an arbitrary curvature profile. The tracks are connected to the central shaft, which rotates in air bushings with low friction. The base of the system is fixed on the hard ground via the kinematic mount, which constrains motion of the base.

We control the motors' positions on the tracks to prescribe a "gait"—a closed path in shape space parameterized by the position of the motor positions in horizontal (θ_h) and vertical (θ_v) directions, as shown in Fig. 1B. The swimmer is constrained to move angularly by the beam arm (Fig. 2A). This design can minimize environmental forces due to friction and gravity, although we also demonstrate that these couple to the geometric phase to generate additional exotic phenomena.

We test whether self-deformation in the presence of curvature can generate locomotion without significant environmental forces. We place the robot on the equator of the sphere and for simplicity, restrict ourselves to shapes that are symmetrical under reflections across the equator. Such shape changes, combined with the apparatus design, constrain the robot to translate along the equator (i.e., to rotate about the north pole). The smooth trajectory through shape space, designed to minimize jerks and maximize motion, is shown in Fig. 1B and further explicated in *SI Appendix, section 2*.

In our primary result, as predicted by Wisdom (7) and indicated in Fig. 1A, the persistent cycling through shape space shown in Fig. 2 B and C leads the robot to translate back and forth,

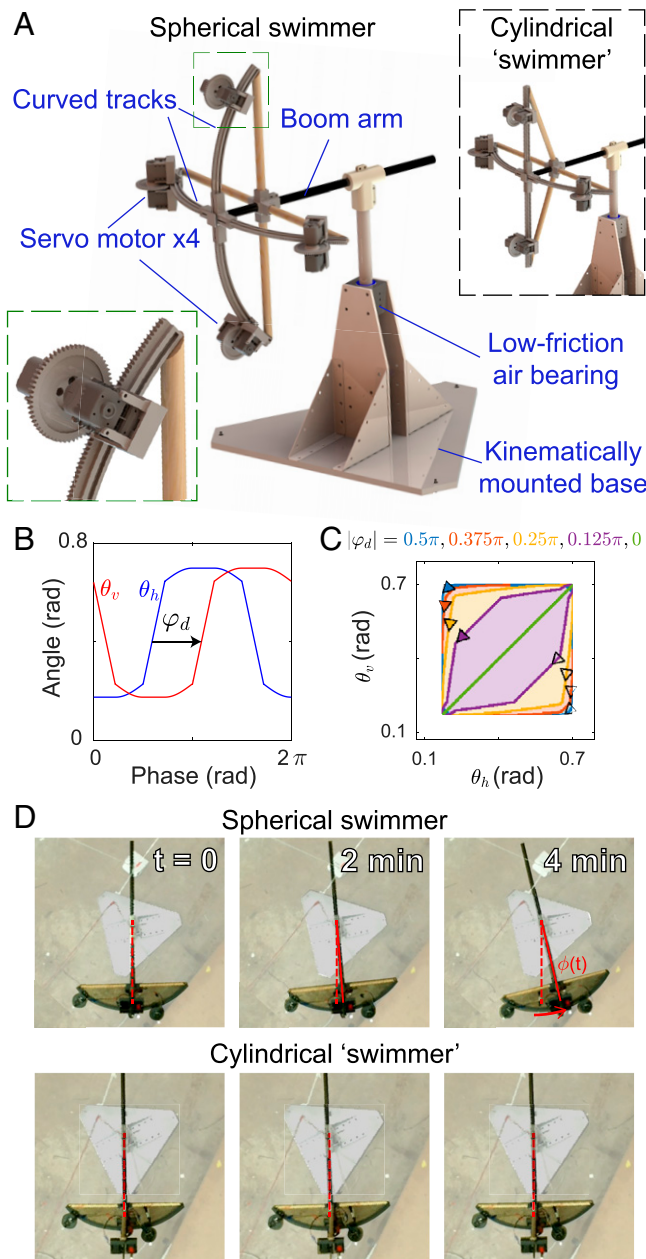


Fig. 2. Robophysical curved space swimmer. (A) The experimental apparatus, rendered here schematically, confines the robot's active masses to a geometric (but not material) spherical surface of radius of 46 cm via 3D-printed curved tracks along which servo motors (116 g for each of the four motors) propel masses of themselves and the tracks (388 g). The robot is free to rotate about a central pivot with a low-friction air bearing and mounted on a kinematically adjustable base used to minimize the torque induced by gravity. In contrast, *Upper Right Inset* depicts a robot that due to the straight arms, is confined to a cylindrical surface along which no corresponding motion can be induced via swimming. *Lower Left Inset* shows the coupling between a motor and a curved track. (B) A phase difference φ_d between the robot's horizontal and vertical strokes breaks time reversal and spatial inversion symmetry, as required for forward swimming. (C) The displacement of the robot per stroke, in the absence of external forces, is obtained as an integral of geometric phase over the shaded regions enclosed by the gaits in shape space. (D) Chronological snapshots of the spherical swimmer and the cylindrical "swimmer" show that the swimming of the former is significant, while the latter is vanishingly small. The red trajectories in Figs. 3A and 4A show the displacement over time, and Movie S1 shows the video of these two experiments.

yet the effect of Gaussian (intrinsic) curvature permits a relatively small net motion (Fig. 3B), which depends on the direction of the cycle in the configuration space. Additionally, as predicted,

because force-free propulsion relies on this curvature of the doubly curved sphere, a robot confined to a singly curved cylindrical surface (Fig. 2A, *Insets*) does not exhibit this propulsion (Figs. 3B and 4A, *Inset*). Further, in contrast to Wisdom's force-free model, the robotic swimmer's motion saturates at a finite displacement, per Fig. 4A.

While we have now realized force-free swimming, as occurs over short times in Fig. 3A, the robophysical testing reveals more complex phenomena resulting from the interplay between this geometric phase and environmental effects, as in Fig. 4A. We now develop an analytical theory and use numerical simulation to rationalize these results. The full equations of motion described in *SI Appendix, section 3* simplify for the equatorial spherical swimmer to the scalar associations between the angular velocity, angular momentum, and torque about the vertical axis, which are our system's instances of the broader concepts of generalized velocity, momentum, and force:

$$\dot{\phi}(t) = \frac{L(t) - \dot{\alpha}(t)}{I(t)}, \quad [1a]$$

$$\dot{L}(t) = \tau(\phi, \dot{\phi}) = -\tau_C \operatorname{sgn} \dot{\phi} - \tau_g \phi. \quad [1b]$$

The moment of inertia $I(t)$ and the internal effective angular momentum $\dot{\alpha}(t)$ both depend on time with period T via the shape-change gait. $I(t)$ is the instantaneous moment of inertia, the inverse ratio of the angular velocity to the angular momentum it would induce. $\dot{\alpha}$, in turn, is the angular momentum that would be present even if the robot was not rotating (note that there is ambiguity in how to distinguish between the robot's changes

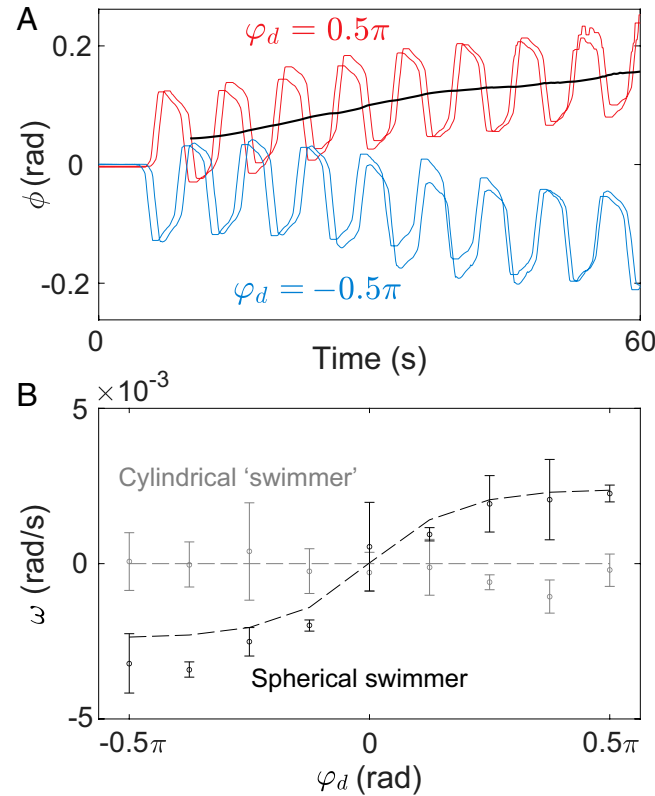


Fig. 3. Self-propulsion via geometric phase. (A) The robot, initially at rest, swims forward with an average initial angular velocity $\omega_i = \dot{\phi}$ over the course of several strokes. The black thick line shows the time-averaged position $\bar{\phi}$. (B) The observed initial velocities match those predicted from the geometric phase (dashed lines), ω_g , with variable gait controlling the speed and direction of the robot swimming on the sphere in contrast to the robot on the cylinder, which cannot achieve significant net movement.

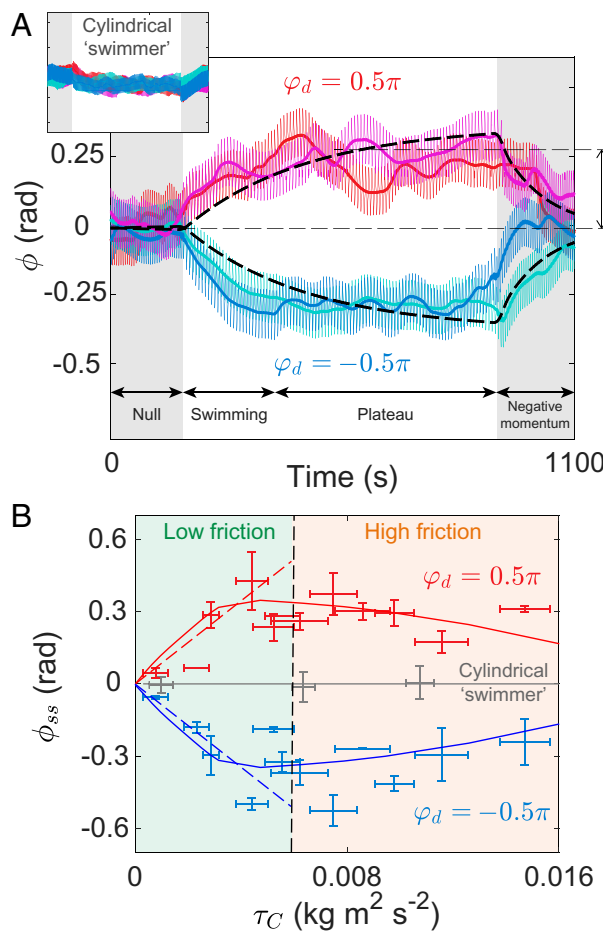


Fig. 4. Geometric swimming in the presence of environmental effects. (A) Evolution of $\phi(t)$ of the curved swimmer and the cylindrical nonswimmer (Inset) for Coulomb friction $\tau_C = 3.4 \times 10^{-3} \text{ kg m}^2/\text{s}^2$ and different φ_d 's (Movie S1). There are two trials for each φ_d . (B) The steady-state plateau ϕ_{ss} as a function of τ_C . The error bars and solid lines show the experiment and simulation (Eq. 1), respectively. To understand how the plateau increases with small friction ($\tau_C < |\ddot{\alpha}|$), we show the first-order theory (Eq. 5) with dashed lines until around the predicted cutoff friction ($\tau_C = |\ddot{\alpha}|$).

in shape and orientation, but any self-consistent choice is valid). Slight misalignment between the axis of the swimmer and gravity leads to a residual gravitational force and hence, a torque $-\tau_g \dot{\phi}$, where $\dot{\phi}$ is measured relative to the gravitational potential minimum. Similarly, friction, specifically Coulomb friction, generates a force opposing motion but approximately independent of speed, leading to the torque proportional to τ_C . These parameters are measured, rather than left as free model parameters, in additional experiments as described in *SI Appendix, sections 4 and 5*.

As a consequence of the dynamics of Eq. 1, even when angular momentum and torque are negligible, as they are for a time when τ_C, τ_g are small, the robot's gait causes it to advance at an average angular velocity:

$$\omega_g = \frac{\Delta\phi}{T} = -\frac{1}{T} \int_0^T I^{-1}(t) \dot{\alpha}(t) dt = -\frac{1}{T} \oint \frac{d\alpha}{I}. \quad [2]$$

The final expression reflects the geometric nature of this movement as a Berry phase that depends on the path through shape space but not on the rate at which it is traversed, which can also be written via Stokes' theorem as a two-dimensional integral of an effective curvature in this abstract shape space. For a general curved surface with axial and mirror symmetry, we find that the direction and magnitude of the swimmer's displacement over one cycle are

dictated by the collective contribution of the surface curvature and the trajectory in the shape space (*SI Appendix, section 8* has details). The swimmer displays positive, zero, and negative translation when executing the same gait on a sphere, a cylinder, and a hyperboloid. Note, however, that even on surfaces for which the Gaussian curvature vanishes almost everywhere, localized defects, such as the point of a cone, can lead to novel dynamics (8). In fully flat spaces, however, the analogous expression for the linear velocity induced by the shape changes vanishes, as the moment of inertia is replaced with the scalar mass, a constant.

Emergent Dynamics with Geometric Phase and External Forces

As posited in Fig. 1 and shown in Fig. 3A, in the absence of additional forces, a robot initially at rest would, upon initiating a particular series of shape changes, rotate around the equator of its spherical universe at a rate described by Eq. 2, a behavior analogous to the general relativistic formulation of Wisdom (7). Instead, we address the complex coupling between this geometrical phase and the robot's coupling to its environment reflected in the torques of Eq. 1.

Perhaps surprisingly, while the geometric phase is evaluated via a nonlinear numerical integration and the Coulomb friction is highly nonlinear, the interplay between the two can be treated analytically. This process, shown in *Two Diverging Friction Models*, is done in the rotating wave approximation, in which drawing inspiration from techniques developed in optical physics (22), we decouple the rapid oscillations of the robot from the weaker influences of external torques:

$$\ddot{\bar{\phi}} = \frac{4\tau_C}{T|\ddot{\alpha}|} \omega_g - \frac{4\tau_C}{T|\ddot{\alpha}|} \dot{\bar{\phi}} - \frac{\tau_g}{\langle I^{(0)} \rangle} \bar{\phi}. \quad [3]$$

$$\dot{L} = -\frac{4\tau_C}{T|\ddot{\alpha}|} L - \tau_g \bar{\phi}. \quad [4]$$

Here, $\bar{\phi}(t)$ is the time-averaged position, removing the rapid, high-amplitude oscillations due to the gait motion, as shown in Figs. 3A and 4. $\langle I^{(0)} \rangle$ is the inverse of the time averaging of the inverse moment of inertia. $\ddot{\alpha}$ is the rate of change of the internal angular momentum at the time in the gait at which it vanishes. This linear approximation relies on the smallness of the external angular momentum L relative to the internal angular momentum $\dot{\alpha}$. For larger angular momenta, higher-order terms become relevant.

We thus arrive at the effective dynamics of the curvature swimmer. Provided that the external torque does not vary significantly within a single stroke and the system remains in the linear force regime, the system attains an emergent form of the viscously damped ($4\tau_C \dot{\bar{\phi}} / T|\ddot{\alpha}|$) linear harmonic oscillation, despite the nonlinearity of the Coulomb friction. The most striking feature is the uniform force field $4\tau_C \omega_g / T|\ddot{\alpha}|$, proportional to both the geometric phase ω_g and the Coulomb friction τ_C . The periodic shape changes are reminiscent of a Floquet theory, yet the combination of a time-dependent force with a time-dependent inertia permits net forward motion.

The low-torque regime occurs when the swimmer, initially at the bottom of a shallow energy well engaged in a neutral swimming motion (which does not lead to self-propulsion but maintains continuous self-deformation to prevent static friction, referred as the null stage in Fig. 4A), shifts into a forward swimming motion, referred as the swimming stage. The swimmer is considered to enter the plateau stage when ϕ transits to its steady

state (the protocol of experimentally determining the transition point is specified in *SI Appendix, section 2*). The robot's motors drive its masses around the spherical surface in the trajectory shown in Fig. 2*B*. The parameter φ_d controls the offset between the motions of the horizontal and vertical arms, which is crucial to break time reversal and spatial inversion symmetries, as is necessary for a swimming gait. Here, we refer to a gait with nonzero φ_d and thus, nonzero swimming as a swimming gait and refer to a gait with zero φ_d as a null gait. *Movie S1* shows demonstrations of the null and swimming gaits and examples of swimming motion for $\varphi_d = \pm\pi/2$. The geometric phase ω_g is shown in Fig. 3. Over short periods, the forces effect only a small change in the swimmer's momentum, while the swimmer nevertheless advances at a measured initial angular rate $\omega_i = \dot{\phi}(0)$. As seen in Fig. 3*B*, the rate predicted (dashed line) by the calculated geometric phase ω_g (i.e., $\omega_i = \omega_g$) is in agreement with the observed initial rate, providing strong validation of the geometric theory.

This analysis identifies a geometric phase in the regime in which the swimming motion is much faster than the natural frequency of the potential. The Hannay angle (23) describes a geometric phase in the opposite regime, in which the swimming motion is much slower than the natural oscillations of the robot in the gravity well and in which the swimming motion would alter the frequency of oscillations. The framework we use in our paper applies more generally to swimmers on curved surfaces, such as the helicoid in *SI Appendix, section 9*, which is a noncompact manifold that permits unbounded locomotion.

Environmental Forces and Momentum without Locomotion

Over longer times, additional vibrations, resonances, and nonlinearities preclude quantitative agreement between experiment and theory, yet qualitative agreement is nevertheless observed throughout the trajectory in Fig. 4*A*. These trajectories contain a surprising feature; unlike the typical behavior of dissipative systems in flat space, the curvature drives the swimmer to plateau at a finite offset from the bottom of its potential well. The geometric theory of Eq. 3 predicts $\tau(\phi_{ss}) = \frac{4\tau_C \langle I^{(0)} \rangle}{T|\ddot{\alpha}|} \omega_g$ and leads to a steady-state plateau of

$$\bar{\phi}_{ss} = \frac{4\tau_C \langle I^{(0)} \rangle}{\tau_g T |\ddot{\alpha}|} \omega_g. \quad [5]$$

This prediction of linear dependence between plateau height and friction strength is observed at low-friction strength, as shown in Fig. 4*B*, and levels off at approximately the amount of friction strength predicted by theory, which is $|\ddot{\alpha}|$ (*SI Appendix, section 7*).

The trajectory in Fig. 4*A* naively suggests that the swimmer begins with a finite momentum that falls to zero as its position plateaus. As our analysis reveals, the reverse is true; at the beginning of the swimmer's journey, when its velocity is greatest, it lacks momentum. In contrast, once its average velocity in one direction vanishes, the momentum is maximal and points in the opposite direction. Because the swimmer advances without momentum, the dissipative forces that arrest the swimmer's forward progress also impart an impulse that leaves it with nonzero momentum. To illustrate this, in Figs. 4*A* and 5, we suspend the swimmer's forward stroke, replacing it with a null gait to prevent static friction. At this moment, normal classical physics, in which momentum and velocity are in proportion to one another, reasserts itself, and the swimmer's negative momentum causes it to swing backward toward its origin. We emphasize that this is not

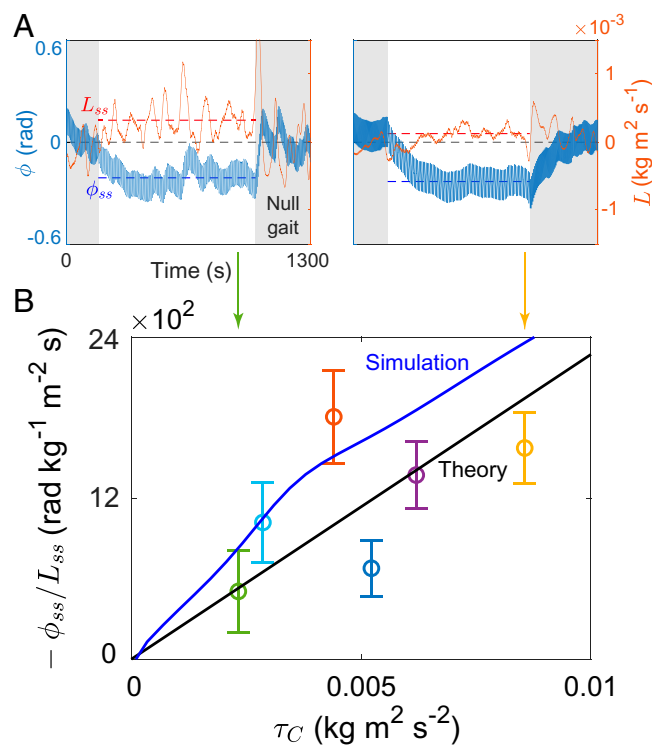


Fig. 5. Negative momentum in the steady state via environmental effects. (A) Simultaneous evolution of ϕ and L for low and high friction ($\tau_C = 0.0023, 0.0089 \text{ kg m}^2 \text{s}^{-2}$) for a swimmer conducting a swimming gait sandwiched by two null gaits. Note that the steady-state plateau ϕ_{ss} and angular momentum L_{ss} have opposite signs. (B) The ratio between the ϕ_{ss} and L_{ss} for various torques of friction τ_C . The black line shows the theory $-\phi_{ss}/L_{ss} = 4\tau_C/(T|\ddot{\alpha}|\tau_g)$ with all parameters measured from experiments. The blue line shows the simulation result.

due to external forces; gravity is weak, and friction opposes this motion. This is due purely to the momentum concealed by and compensated for in the swimmer's gait. The curvature swimmer thus displays the exotic behavior of using dissipative (frictional) forces to increase the magnitude of its momentum in the rest frame of its environment. This relationship between steady-state displacement and momentum remains in qualitative agreement with simulation and theory (without free parameters) as friction is varied.

Conclusions

In summary, we have experimentally realized and theoretically characterized the movement of a robot through a curved (spherical) space without relying on any momentum or reliance on environmental forces to translate, in contrast with all other observed systems. We demonstrated that this purely geometric effect couples to both conservative and dissipative forces present in real environments. In particular, we have shown how coupling between Coulomb friction and the geometric phase generates an emergent effective force on the robot that imparts an impulse that reduces its velocity while increasing its momentum in the opposite direction. This behavior sheds light both on Wisdom's proposed locomotion via space-time curvature (7) and more immediately, on a geometric effect always present when robots move on curved surfaces. Note that despite the curvature, the space considered here is homogeneous and isotropic. In contrast, a stressed structure experiences forces dependent on gradients of curvature (5), and this effect may be used in conjunction with the present phenomena to generate locomotion schemes. As shown

here, this effect can become dominant when the robot's body is comparable with the inverse curvature of the surface, which appears to extend to gravitational curvature of space-time as well (7). Further, the apparatus presented here can function as a test bed for additional exotic behavior on curved surfaces, related to more complex and variable swimming gaits, nonlinear effects, and collective behavior.

Materials and Methods

Experiment Apparatus. The swimmer is composed of four controlled motor modules functioning as moving masses on four curved and toothed tracks 3D printed with polylactic acid filament; the motors couple to the tracks via gears that fit within the tracks' teeth and allow rolling without slipping. The four tracks as shown in Fig. 2A are mounted to a horizontal carbon fiber beam arm. This arm is attached to a vertical steel shaft, which can rotate about the z axis. To create a low-friction environment for the swimmer, the steel shaft is supported by two air bearings and one air bushing.

The apparatus is attached to a kinematically mounted base, which allows for leveling of the swimmer to within 10^{-4} radian. To vary friction to systematically slow the swimmer and probe environmental interaction effects, we attach a block of polyurethane foam to a screw-adjusted sliding block, allowing for adjustable normal contact between the shaft and the foam.

Motion of servo motors (Dynamixel AX-12A; Robotis) is controlled by position commands from a microcontroller. The instantaneous motion of the swimmer and the positions of individual motors over time are recorded by an optical tracking system (Optitrak) via IR (infrared) reflective markers attached to the motors.

More details of the apparatus are in *SI Appendix, section 1*.

Numerical Integration. We implement the same gait as the commanded shape change sent to the motors by interpolating these discrete signals in the differential equations. To lower the computation cost of interpolation, we use a numerical scheme with fixed steps (forward Euler). The test of convergence with step size h shows a global error (i.e., the error in the position ϕ) of $O(h)$ [and therefore, local error of $O(h^2)$] as expected for a first-order scheme. We use the step size $h = 3.1 \times 10^{-4}$ s such that the relative error is 1.8 %. *SI Appendix, section 6* has the details.

Shape Dynamics. As described in the text, we consider a robot undergoing shape changes while confined to a spherical surface of radius R_0 . Here, we describe some of the technical details of the general formulation.

Let our robot's shape $S(t)$ be described by masses m_i at points $R_0\hat{s}^{(i)}(t)$. We choose units such that we can set the radius to one. In the case of a continuous robot, we would need to define some other sets of degrees of freedom to parameterize the shape of the robot. From the general definition that angular momentum is the cross-product of position with momentum, the shape change alone induces an angular momentum:

$$\sum_i m_i \hat{s}^{(i)} \times \partial_t \hat{s}^{(i)}. \quad [6]$$

However, the dynamics will also select some rigid rotation of the robot, $\mathbf{R}(t)$. This will not only rotate the above contribution but generate a new term, as the position of mass i is $\mathbf{R}(t)\hat{s}^{(i)}(t)$ and its velocity is $\dot{\mathbf{R}}\hat{s}^{(i)} + \mathbf{R}\partial_t \hat{s}^{(i)}$. Hence, the angular momentum is

$$\mathbf{L} = \sum_i m_i (\mathbf{R}\hat{s}^{(i)}) \times (\dot{\mathbf{R}}\hat{s}^{(i)} + \mathbf{R}\partial_t \hat{s}^{(i)}) \quad [7]$$

$$= \sum_i m_i (\mathbf{R}\hat{s}^{(i)}) \times \mathbf{R} (\mathbf{R}^{-1}\dot{\mathbf{R}}\hat{s}^{(i)} + \partial_t \hat{s}^{(i)}) \quad [8]$$

$$= \mathbf{R} \sum_i m_i \hat{s}^{(i)} \times (\mathbf{R}^{-1}\dot{\mathbf{R}}\hat{s}^{(i)} + \partial_t \hat{s}^{(i)}). \quad [9]$$

We recognize the term $\mathbf{R}^{-1}\dot{\mathbf{R}}$ as an element of a Lie algebra. It is the skew-symmetric generator of infinitesimal rotations. When the angular momentum

in rotated coordinates, the shape, and the shape change are all known, this generator may always be solved for. One may then integrate these generators numerically to obtain the total rotation induced by a set of shape changes. As shown by Shapere and Wilczek (10) for general rigid-body rotations, in the limit of small shape changes (e.g., a robot small compared with the radius of curvature), this may be expressed as a gauge theory.

However, in order to achieve a more experimentally accessible regime, we must impose large shape changes, in which the robot evolves over length scales comparable with the inverse curvature (i.e., radius) of the space in which it lies. In order to generate an analytically tractable theory, we then restrict ourselves to shapes that are symmetrical under reflections about the equator. Consequently, the final term in the angular momentum expression above must point in the z direction. It also follows that the linear operator acting on the generator of rotations is symmetric about this reflection as well. Therefore, in the absence of external forces to the contrary (our robot is fixed to the equator, preventing gravity from breaking this symmetry and drawing it to the south pole) for a robot initially at zero angular momentum, all rotations must be about the vertical axis. This leads to the following expression for the remaining component of angular momentum:

$$\hat{\mathbf{L}} = \left[\sum_i m_i \hat{s}^{(i)} \times (\hat{z} \times \hat{s}^{(i)}) \right] \dot{\phi}(t) + \sum_i m_i \hat{s}^{(i)} \times \partial_t \hat{s}^{(i)}, \quad [10]$$

$$L \equiv I(t)\dot{\phi}(t) + \dot{\alpha}(t). \quad [11]$$

The coefficient of $\dot{\phi}(t)$ is the zz component of the moment of inertia tensor, which is denoted $I(t)$. The final term, which we denote $\dot{\alpha}$, is the angular momentum the robot would have due to its shape change even if it were not rotating. For example, if the base of the robot is fixed but one of its legs is proceeding counterclockwise, it would have counterclockwise angular momentum. $\dot{\alpha}(t)$ is periodic for periodic movements of masses. For the movements we consider, $\dot{\alpha}(t)$ is antisymmetric about a point due to the relevant mass moving forward and backward in the same manner. As such, $\int_0^T \dot{\alpha}(t) dt = 0$, and $\alpha(t)$ is also periodic. However, the geometric phase of Eq. 2 depends only on $d\alpha$ and not $\alpha(t)$ itself, and consequently, the geometric phase would be the same in each period even if $\alpha(t)$ was not itself periodic. One advantage of this formulation in terms of moment of inertia and angular momentum is that it provides a universal language that applies regardless of the particular shapes a robot passes through.

Calculating Berry Phases and Applying the Rotating Wave Approximation. As discussed in the previous section and the text, we have an equation of motion describing how the angular momentum and internal shape changes induce changes in the robot's position,

$$\dot{\phi}(t) = \frac{L(t) - \dot{\alpha}(t)}{I(t)}, \quad [12]$$

and one governing how external forces modify the angular momentum,

$$\dot{L} = \tau(\phi, \dot{\phi}). \quad [13]$$

Here, we discuss how an approximate theory emerges under mild assumptions that are well satisfied in practice. We assume that the angular momentum is varying fairly slowly relative to the timescale of the robot's gait, so that we might expand it as $L(t) \approx L(t_0) + (t - t_0)\dot{L}(t_0) + \dots$. We also assume that the moment of inertia is time symmetric about $t = 0$, although note that this does not imply that the gait as a whole is time symmetric (a fully time-symmetric gait could not advance in any direction, at least barring spontaneous symmetry breaking). Now, let us define the n th moment as

$$\langle L^{(n)} \rangle^{-1} \equiv T^{-(n+1)} \int_{-T/2}^{T/2} dt t^n L(t)^{-1}. \quad [14]$$

In these terms, using the fact that odd moments vanish by symmetry, we have that over one period, the time-averaged change in angular position is

$$\dot{\phi} = -\frac{1}{T} \oint \frac{d\alpha}{I} + \frac{L}{\langle L^{(0)} \rangle} + \frac{T^2}{2\langle L^{(2)} \rangle} \ddot{\alpha} + O(T^4). \quad [15]$$

That is, to good approximation, the advancement of the robot is given by the geometric phase plus the term one would expect in the absence of shape changes: the angular momentum divided by a time averaging of the moment of inertia. Corrections to this picture emerge as the angular momentum changes rapidly over a single stroke of the gait.

Even ignoring these higher-order terms, the portion of the angular position that is not time averaged may have a substantial amplitude, as indeed is observed in our experimental system.

Two Diverging Friction Models. Consider a simple model of viscous friction and a conservative force:

$$\dot{L} = -\eta \dot{\phi} + \tau(\phi). \quad [16]$$

This time averages trivially to

$$\dot{L} \approx -\eta \dot{\bar{\phi}} + \tau(\bar{\phi}). \quad [17]$$

By combining this expression with the dominant terms in Eq. 15 (after time differentiating), we have

$$\langle L^{(0)} \rangle \ddot{\bar{\phi}} = -\eta \dot{\bar{\phi}} + \tau(\bar{\phi}). \quad [18]$$

These dynamics now resemble those of typical oscillator motion. Indeed, the geometric phase has vanished. Its relevance comes in returning to Eq. 15, in which we see that for a system that is initially not swimming and at rest (angular momentum zero), the initiation of the swimming motion leads to an initial velocity proportional to the geometric phase, which appears as the first term on the right-hand side of Eq. 15. In the absence of any force, the swimmer would persist at this speed, consistent with Wisdom's picture (7). When viscous friction is included without force, we see that we have trajectories

$$\bar{\phi}(t) = \bar{\phi}(0) + \frac{\langle L^{(0)} \rangle}{\eta} \left[-\frac{1}{T} \oint \frac{d\alpha}{I} \right] \left[1 - \exp \left(-\frac{\eta}{\langle L^{(0)} \rangle} t \right) \right]. \quad [19]$$

At steady state, then we have

$$\Delta \phi_{ss} = \frac{\langle L^{(0)} \rangle}{\eta} \left[-\frac{1}{T} \oint \frac{d\alpha}{I} \right], \quad [20]$$

$$\dot{\bar{\phi}}_{ss} = 0, \quad [21]$$

$$L_{ss} = \frac{\langle L^{(0)} \rangle}{T} \oint \frac{d\alpha}{I}. \quad [22]$$

That is, initially the system has a velocity, given by the geometrical phase, with no momentum. Eventually, its velocity vanishes, but its momentum is nonzero and points in the opposite direction from its previous velocity.

If we include a conservative force, steady state instead requires that the conservative force vanishes, returning the swimmer to the bottom of the potential well. Thus, its geometric phase represents only a temporary escape before it reaches the same fate as a conventional particle driven to the bottom of a potential well by dissipative forces.

We turn then to a different friction model, one that couples more deeply to the geometric phase and that is more relevant to the experimental apparatus—Coulomb friction:

$$\dot{L} = -\tau_C \operatorname{sgn} \dot{\phi} + \tau(\phi). \quad [23]$$

Here, time averaging leads to a different result. Our original gait, by symmetry, has velocity forward as often as backward, with the swimmer advancing because it moves forward more quickly than it moves backward. Thus, any forces resulting from the Coulomb friction come from the potential for angular momentum to

change the fraction of the time it spends going forward. The average value of the Coulomb friction term is, then,

$$\dot{L} \approx -\frac{4\tau_C}{T} \left(\dot{\alpha}^{-1}(L) - \dot{\alpha}^{-1}(0) \right) + \tau(\bar{\phi}). \quad [24]$$

Here, the term $\dot{\alpha}^{-1}(L)$ appears because per Eq. 12, the periods in which the velocity is positive end and begin with periods in which $\dot{\alpha}(t) = L$. The factor of four occurs because this effect at the beginning of such a period is mirrored, by symmetry, with the opposite effect at the end of the period and because as the period in which this term is positive increases, the period in which it is negative decreases.

Because $\dot{\alpha}(t)$ is odd about one of its zeros, in expanding the above equation we do not obtain $O(L^2)$ terms. Higher-order terms can be neglected, leading to

$$\dot{L} \approx -\frac{4\tau_C}{T|\ddot{\alpha}|} L + \tau(\bar{\phi}). \quad [25]$$

Here, $\ddot{\alpha}$ is evaluated at one of the zeroes of $\dot{\alpha}$. The result is something resembling again viscous friction. However, for our system, the distinction between a term proportional to angular momentum and one proportional to angular velocity is profound.

Indeed, upon combining this equation with Eq. 15 and again, suitable time derivatives, we obtain the equations of motion for the Coulomb friction case:

$$\langle L^{(0)} \rangle \ddot{\bar{\phi}} = -\frac{4\tau_C \langle L^{(0)} \rangle}{T|\ddot{\alpha}|} \left[\dot{\bar{\phi}} + \frac{1}{T} \oint \frac{d\alpha}{I} \right] + \tau(\bar{\phi}). \quad [26]$$

That is, in the time-averaged dynamics, the Coulomb model leads to a viscous-like term but also, to a uniform forcing term from the interaction between the geometric phase and the Coulomb friction. This leads to strikingly different dynamics than in the viscous case.

In particular, in the absence of the conservative force, the Coulomb curvature swimmer advances forever, reaching a steady state in which angular momentum vanishes but velocity is given by the geometric phase:

$$\dot{\bar{\phi}}_{ss} = -\frac{1}{T} \oint \frac{d\alpha}{I}. \quad [27]$$

Moreover, in the presence of a conservative potential well, rather than falling to the bottom, the swimmer is able to reach a steady state in which the interaction between the Coulomb potential and the geometric phase allows the swimmer to resist the conservative force:

$$\tau(\bar{\phi}_{ss}) = \frac{4\tau_C \langle L^{(0)} \rangle}{T^2 |\ddot{\alpha}|} \oint \frac{d\alpha}{I}. \quad [28]$$

Data Availability. All datasets are available at <https://smartech.gatech.edu/handle/1853/66809> (24).

ACKNOWLEDGMENTS. We thank Baxi Chong, Andras Karsai, Bo Lin, Jack Wisdom, and Lutian Zhao for advice and discussion. Funding for S.L., T.W., V.H.K., J.M., E.A., Y.O.-A., D.I.G., and D.Z.R. was provided by Army Research Office Contract W911NF-19-1-0056; funding was also provided to D.I.G. by a Dunn Family Professorship.

Author affiliations: ^aSchool of Physics, Georgia Institute of Technology, Atlanta, GA 30332; ^bInstitute for Robotics and Intelligent Machines, College of Computing, Georgia Institute of Technology, Atlanta, GA 30332; ^cSchool of Mechanical Engineering, Georgia Institute of Technology, Atlanta, GA 30332; ^dDepartment of Physics, University of Michigan, Ann Arbor, MI 48109; ^eCollege of Engineering, University of Notre Dame, Notre Dame, IN 46556; and ^fDepartment of Electrical Engineering, University of Notre Dame, Notre Dame, IN 46556

1. R. E. Guerra, C. P. Kelleher, A. D. Hollingsworth, P. M. Chaikin, Freezing on a sphere. *Nature* **554**, 346–350 (2018).
2. T. Lopez-Leon, V. Koning, K. Devaiah, V. Vitelli, A. Fernandez-Nieves, Frustrated nematic order in spherical geometries. *Nat. Phys.* **7**, 391–394 (2011).
3. Y. H. Zhang, M. Deserno, Z. C. Tu, Dynamics of active nematic defects on the surface of a sphere. *Phys. Rev. E* **102**, 012607 (2020).
4. P. W. Ellis *et al.*, Curvature-induced defect unbinding and dynamics in active nematic toroids. *Nat. Phys.* **14**, 85–90 (2018).
5. H. Aharoni, J. M. Kolinski, M. Moshe, I. Meirzada, E. Sharon, Internal stresses lead to net forces and torques on extended elastic bodies. *Phys. Rev. Lett.* **117**, 124101 (2016).
6. C. W. Misner, K. S. Thorne, J. A. Wheeler, *Gravitation* (Macmillan, 1973).
7. J. Wisdom, Swimming in spacetime: Motion by cyclic changes in body shape. *Science* **299**, 1865–1869 (2003).

8. J. Avron, O. Kenneth, Swimming in curved space or the baron and the cat. *New J. Phys.* **8**, 68 (2006).
9. E. Guérin, Adventures in curved spacetime. *Sci. Am.* **301**, 38–45 (2009).
10. A. Shapere, F. Wilczek, Gauge kinematics of deformable bodies. *Am. J. Phys.* **57**, 514–518 (1989).
11. J. E. Marsden, J. Ostrowski, “Symmetries in motion: Geometric foundations of motion control” in *Motion, Control, and Geometry: Proceedings of a Symposium*, A. Friedman, Ed. (National Academies Press, Washington, DC, 1998), pp. 3–19.
12. S. D. Kelly, R. M. Murray, Geometric phases and robotic locomotion. *J. Robot. Syst.* **12**, 417–431 (1995).
13. R. L. Hatton, Y. Ding, H. Choset, D. I. Goldman, Geometric visualization of self-propulsion in a complex medium. *Phys. Rev. Lett.* **110**, 078101 (2013).
14. R. L. Hatton, H. Choset, Nonconservativity and noncommutativity in locomotion. *Eur. Phys. J. Spec. Top.* **224**, 3141–3174 (2015).
15. H. C. Astley *et al.*, Surprising simplicities and syntheses in limbless self-propulsion in sand. *J. Exp. Biol.* **223**, jeb103564 (2020).
16. B. Chong *et al.*, Frequency modulation of body waves to improve performance of sidewinding robots. *Int. J. Robot. Res.* **40**, 1547–1562 (2021).
17. J. Hannay, Swimming holonomy principles, exemplified with a Euler fluid in two dimensions. *J. Phys. A Math. Theor.* **45**, 065501 (2012).
18. P. Saffman, The self-propulsion of a deformable body in a perfect fluid. *J. Fluid Mech.* **28**, 385–389 (1967).
19. H. G. Yevick, G. Duclos, I. Bonnet, P. Silberzan, Architecture and migration of an epithelium on a cylindrical wire. *Proc. Natl. Acad. Sci. U.S.A.* **112**, 5944–5949 (2015).
20. S. Shankar, M. J. Bowick, M. C. Marchetti, Topological sound and flocking on curved surfaces. *Phys. Rev. X* **7**, 031039 (2017).
21. S. Li *et al.*, Field-mediated locomotor dynamics on highly deformable surfaces. *Proc. Natl. Acad. Sci. U.S.A.* **119**, e2113912119 (2022).
22. E.T. Jaynes, F.W. Cummings, Comparison of quantum and semiclassical radiation theories with application to the beam maser. *Proc. IEEE* **51**, 89–109 (1963).
23. J. H. Hannay, Angle variable holonomy in adiabatic excursion of an integrable Hamiltonian. *J. Phys. Math. Gen.* **18**, 221 (1985).
24. S. Li *et al.*, Data for ‘Locomotion without force, and impulse via dissipation: Robotic swimming in curved space via geometric phase.’ Georgia Institute of Technology. <https://smartech.gatech.edu/handle/1853/66809>. Deposited 22 June 2021.